Hindawi
International Journal of Polymer Science
Volume 2019, Article ID 7103936, 12 pages
https://doi.org/10.1155/2019/7103936

Research Article

Nanocrystalline Cellulose/Polyvinylpyrrolidone Fibrous Composites Prepared by Electrospinning and Thermal Crosslinking

Katrina M. Hatch,[1] Jana Hlavatá,[2] Katherine Paulett,[1] Tatsiana Liavitskaya,[3] Sergey Vyazovkin,[3] and Andrei V. Stanishevsky[1]

[1]*Department of Physics, University of Alabama at Birmingham, 1300 University Boulevard, Birmingham, AL 35294, USA*
[2]*Faculty of Textile Engineering, Technical University of Liberec, Studentska 2, Liberec 1 461 17, Czech Republic*
[3]*Department of Chemistry, University of Alabama at Birmingham, 901 14th Street South, Birmingham, AL 35294, USA*

Correspondence should be addressed to Andrei V. Stanishevsky; astan@uab.edu

Received 30 November 2018; Revised 5 February 2019; Accepted 18 February 2019; Published 27 March 2019

Academic Editor: Huining Xiao

Nanocellulose/polyvinylpyrrolidone (nCel/PVP) fibrous composite materials containing rod-like nanocrystalline cellulose particles with the lengths varying in the range from 100 to 2000 nm were prepared by using DC electrospinning. The particle size had a strong effect on the precursor viscosity, process efficiency, and resulting fiber diameter. The thermal crosslinking of nCel/PVP composite nanofibers with up to 1.0 : 8.0 nCel/PVP weight ratio resulted in fibrous membranes with textural, air transport, and mass swelling properties varying significantly with the size of cellulose particles. The presence of nCel particles increased the oxidation resistance of PVP during the crosslinking and affected the morphological changes of nCel/PVP fibrous membranes in aqueous solutions. Particles with the smallest size improved the strength of the membrane but decreased its mass swelling capacity, whereas the larger particles led to a more porous and flexible, but mechanically weaker, membrane structure with a higher swelling ability. Thus, by using the nCel particles of different size and shape, the properties of nCel/PVP composite fibrous membranes can be tailored to a specific application.

1. Introduction

Nanocellulose (nCel), in its nanocrystalline, microfibrillar, or bacterial cellulose form, has advanced as a key component in a variety of biomedical materials intended for drug delivery, wound dressings, biomedical implants, vascular grafts, and scaffolds for tissue engineering [1–3]. It has been a popular topic in research due to its physical properties, biocompatibility, biodegradability, and low toxicity.

Nanocellulose particles have also been increasingly used as an additive to many natural and synthetic polymers to create new composite materials with improved service characteristics and new combinations of useful properties [4]. The addition of nanocellulose particles has recently been shown to improve the mechanical properties of polymer fibers produced by the electrospinning process. This process uses a high electric field to generate electrically charged jets of polymer solutions to produce micro- and nanofibers [5, 6]. Electrospun fibrous polymer materials have been found to be advantageous for many biomedical, environmental, and other applications [7, 8].

Most of the research conducted on electrospun nCel particle-loaded composite polymer fibers has been focused on the development of a fabrication process, the fiber structure and morphology analysis, and tensile tests of fibrous assemblies. For example, the addition of nanocellulose particles to a polymer precursor solution has been shown to improve the tensile modulus and strength of polyvinyl alcohol (PVA) [9, 10], poly(ethylene oxide) (PEO) [11], polylactic acid (PLA) [12–15], polycaprolactone (PCL) [16–18], polylactic-co-glycolic acid (PLGA) [19], and polyacrylonitrile (PAN) [20] electrospun fibrous materials. It has been

noted that the effect of nanocellulose depends strongly on the polymer matrix and amount of nanocellulose added. For example, a remarkable 22-fold increase in the tensile modulus and 5-fold increase in strength has been reported [15] for electrospun PLA nanofibrous mats upon the addition of 5 wt% of nCel rod-like particles with the lengths ranging from 40 to 120 nm and an average diameter of 8.7 ± 1.7 nm. It was also found that the increase in nanocellulose content could lead to faster biodegradation of the composite nanofibrous material. In most of the other published reports, a rather moderate improvement in mechanical properties of nCel/polymer fibrous composites has been observed. Mo et al. [19] noted that the incorporation of 7 wt% of bacterial nanocellulose into the PLGA precursor solution made the mechanical properties of electrospun nCel/PLGA fibrous composite material comparable with those of natural skin. Another research group [9] found roughly a two-times increase in tensile modulus of nCel/PVA fibrous membranes with up to 20 wt% nanocellulose, but 3.5-times decrease in elongation at break while the tensile strength was not much affected. It was proposed that nCel hinders the normal conformations of polymer chains and inhibits the crystallization of PVA. Other researchers [21] observed similar trends in the mechanical properties and crystallinity of electrospun PVA fibrous materials with up to 15 wt% nanocellulose particles of 3–10 nm in width and up to 250 nm in length.

Several groups reported on preparation of nCel/PVP fibers by electrospinning for possible applications as antibacterial [22], enhanced stiffness [23], and efficient air filtration materials [24]. For example, Going et al. [23] prepared 50 μm thick nCel/PVP fibrous mats loaded with needle-like nanocellulose particles with the lengths of 50–90 nm and widths of 4.4–8.2 nm. It was shown that the addition of nCel particles strongly increases the viscosity of precursor solution, but it was still possible to fabricate nCel/PVP fibrous mats with up to 1.0 : 5.0 nCel/PVP weight ratio. The average diameters of composite fibers were between 385 and 484 nm, and there was little effect of precursor viscosity on the fiber diameter observed. Increased tensile modulus but lower elongation at break and ultimate tensile strength of composite material with 5–10 wt% of nCel were observed in comparison with electrospun pure PVP. Although the decreased total porosity of the composite material should lead to higher strength, it was proposed that nCel particles above some level of loading can serve as stress concentrators which lead to failure at lower loads. In another study, Huang et al. [22] observed that nCel/PVP fibrous mats with 4 wt% or less of similarly sized needle-like nanocellulose particles become stronger but more brittle than pure PVP fibrous mats. It was also noted that the addition of nCel leads to smaller fiber diameters at 2 and 4 wt% nCel loading despite higher viscosity of precursor solutions. The effects of nanocellulose addition and electrospinning process parameters on the nCel/PVP composite fiber diameters were explored by Balgis et al. [24]. It has been proposed that a high negative zeta potential of nanocellulose affects the nCel particle distribution in the composite material and influences the fiber formation during electrospinning. This can, in part, be a concentration-dependent phenomenon which can influence many properties of nCel particle-loaded fibrous composite structures.

The nCel/PVP fibrous composite is a particularly interesting system because PVP, when crosslinked, is a promising material in wound dressing, drug delivery hydrogels, and pervaporation membranes [25–30]. Crosslinked PVP (crospovidone) is also a competitor to cellulose as a filler in medications to facilitate drug delivery [31–33]. The addition of nanocellulose particles to PVP could tailor the mechanical properties and swelling capacity of pure PVP hydrogels and expand the application range. However, dependent upon the source of the cellulose and the treatment it undergoes, the cellulose nanoparticles can vary greatly in their properties, including surface chemistry, morphology, size, chemical group interactions, degree of crystallinity, and aggregation [34, 35]. These factors can determine the particle behavior in the polymer blends and affect the properties of the resulting electrospun fibrous composites. The effect of cellulose particle size and shape on the fabrication process and properties of electrospun composite materials, in particular, nCel/PVP fibrous composite, has not yet been explored. Besides, in previously published reports, the electrospun nCel/PVP composite fibrous materials were not crosslinked.

In the present study, nCel/PVP fibrous materials with nanocellulose particles of different sizes were prepared by using DC electrospinning and thermal crosslinking. The purpose of this study was to investigate the effect of particle size on the nCel/PVP precursor viscosity and spinnability, as well as resulting fiber diameter and morphology, and to provide an initial evaluation of the mechanical integrity and textural and transport properties of nCel/PVP crosslinked composite fibrous membrane structures.

2. Materials and Methods

2.1. Raw Materials. Polyvinylpyrrolidone (PVP, M_w 1,300,000, Sigma-Aldrich, St. Louis, MO, USA) was used as the polymer carrier for the preparation of nanofibers. Ethanol (200 proof) originated from DeconLabs Inc. (King of Prussia, PA, USA). Deionized (DI) water was prepared on site. Samples of nanocellulose (crystallinity index 80–83% as determined by Segal et al.'s method [36]) in the forms of aqueous suspensions or gel were provided by Blue Goose Biorefineries Inc. (Saskatoon, Saskatchewan, Canada). Nanocellulose was produced from the acetate-grade dissolving pulp of western hemlock through a Renewable Residuals Refining (R3)™ oxidative nanocatalytic process that does not involve acid hydrolysis. The parameters of nanocellulose samples of three types—"ultra," "natural," and "thick"—according to the manufacturer's specifications and on-site analysis are summarized in Table 1.

2.2. Precursor Preparation. PVP was dissolved in ethanol to prepare the solution with up to 15 wt% concentration. Nanocellulose was used in its as-received form at 7.4 wt% concentration. When 10 mL of PVP solution and 2.5 mL of nanocellulose solution were mixed together; this resulted in a precursor solution with a 1.0 : 8.0 nCel/PVP weight ratio and 12 wt% concentration with respect to PVP in

Table 1: Properties of the commercial nanocellulose samples.

Cellulose type	State	Particle length (TEM/SEM), nm	Particle diameter (TEM/SEM), nm	Hydrodynamic diameter (DLS), nm	Zeta-potential (Malvern Zetasizer), mV	Electric conductivity, μS/cm (for 7.4 wt% in water)	Carboxyl content (mmol/kg)
BGB "Thick"	Suspension	700–2000	100–220	1232	-36.7	357	177
BGB "Natural"	Thick suspension	400–1200	80–120	566	-36.7	286	140
BGB "Ultra"	Translucent gel	100–200	10–30	104	-32.0	369	150

the 80 : 20 ethanol/water-mixed solvent. The precursors with 10 and 8 wt% PVP concentrations were prepared by diluting the 12 wt% precursor with appropriate amounts of 80 : 20 ethanol/water mixture. All precursors were stirred for up to 48 hours using a magnetic stirrer at 1000 rpm at room temperature.

2.3. Electrospinning and Crosslinking. A capillary needle DC-electrospinning system included a KDS-101 syringe pump (KD Scientific, Hollison, MA, USA) with a 5 mL plastic syringe directly connected to a 19-gauge capillary needle. The positive terminal of either a 40 kV (Gamma High Voltage Research Inc., Ormond Beach, FL, USA) or a 50 kV (Glassman SL150, Glassman High Voltage, High Bridge, NJ, USA) regulated power supply was attached to the needle. A grounded collector was placed 150 mm away from the needle. The needle was connected to a positive terminal of power supply. Generated fibers were deposited on aluminum or copper foil attached to the collector. The fibers were generated at a flow rate typically in the range of 1.0–2.0 mL/h, and the DC voltage varied from 10 kV to 15 kV.

The resulting fibrous sheets were removed from the collector and thermally crosslinked at 200°C for 1 hour in air using a programmable furnace (Isotemp, Fisher Scientific, heating rate 2°C/min).

2.4. Analysis

2.4.1. X-Ray Diffraction. PANalytical Empyrean X-ray diffractometer (PANalytical, Almelo, Netherlands) with a Cu Kα tube (wavelength 0.15406 nm) operating at 45 kV and 40 mA was used to check the crystallinity and phase composition of the nanocellulose precursor. The detector was scanned between 5° and 70°, with a constant takeoff angle of 5°. The size of ordered domains was determined from the Scherrer equation.

2.4.2. Viscosity. To test the viscosity, a HAAKE™ RotoVisco™ 1 Rotational Rheometer (Thermo Scientific, Waltham, MA, USA) in a parallel plate configuration, paired with RheoWin 4 Job and Data Manager Software, was employed. The instrument was programmed to calibrate the zero point before each sample test. Once calibrated, between 0.2 and 3.0 mL of the precursor was used in each test, depending on the apparent viscosity of the sample. All tests were performed in triplicate at 20°C. Apparent viscosity as a function of time was measured at steady shear rate of 1000 s^{-1} over a time period of 120 seconds. To determine the response of the precursor to shear stress, the samples were tested at a varied shear rate from 10 to 1000 s^{-1}. The dynamic viscosity graphs and recorded values were stored within the RheoWin 4 Data Manager and could be exported for further analysis.

2.4.3. Morphology of PVP and nCel/PVP Fibers. The size, shape, and surface morphology of nanofibers were investigated by scanning electron microscopy (SEM, FEI Quanta 650 FE-SEM, Thermo Fisher Scientific, Waltham, MA, USA). SEM imaging was done in secondary electron mode, with an accelerating voltage of 15 kV, an electron probe current of 2 μA, and a chamber pressure of 1×10^{-4} Pa. Diameter analysis of SEM images of each sample was done manually by using ImageJ, an open-source image processing program. Diameters were recorded for at least 50 representative (not fused) fibers in three images taken in different locations for each sample.

2.4.4. Chemical Composition of PVP and nCel/PVP Fibers. Fourier transform infrared spectra (ALPHA FTIR with Eco ATR module, Bruker Optics, Billerica, MA, USA) were acquired from the nanofiber samples positioned in the focal point of the IR beam path to test the chemical composition. In all cases, the FTIR spectra represented an average of 32 scans recorded with a resolution of 2 cm^{-1} for each sample.

2.4.5. Thermal Analysis of PVP and nCel/PVP Fibers. All calorimetric measurements were taken with a heat flux differential scanning calorimeter (DSC) (Model 822e, Mettler Toledo, Columbus, OH, USA). Indium and zinc standards were used to perform temperature, heat flow, and tau-lag calibrations. The experiments were carried out in the atmosphere of nitrogen flow (80 mL min^{-1}). The samples of 7–12 mg were placed in 40 μL aluminum pans with pierced lids. The first heating segment was performed from 25 to 200°C at 10°C min^{-1}, which was followed by cooling to 25°C. The second heating run was carried out from 25 to 200°C at 20°C min^{-1}.

2.4.6. Porosity. Porosity of the as-prepared and dried pure PVP and nCel/PVP fibrous samples was estimated according to the formula

$$P_{\text{dry}} = \left(1 - \frac{\rho_{\text{bulk}}}{\rho_{\text{comp}}}\right) \times 100\%, \quad (1)$$

where ρ_{bulk} is the bulk density of the fibrous mat and $\rho_{\text{comp}} = 1.29$ g/cm^3 is the calculated density of the nCel/PVP fibrous composite material with a 1 : 8 weight ratio of the components. The composite density was calculated using

the reported densities of cellulose $\rho_{cel} = 1.5\,g/cm^3$, and PVP $\rho_{pvp} = 1.26\,g/cm^3$.

Porosity of fibrous samples in equilibrium wet state (achieved normally after two hours of the sample's immersion in water) was calculated according to

$$P_{wet} = \left(\frac{m_{wet} - m_{dry}}{\rho_{water} V_{sample}}\right) \times 100\%, \quad (2)$$

where m_{wet} and m_{dry} are the masses of the nCel/PVP fibrous mat in dry and wet state, ρ_{water} is the mass density of water, and V_{sample} is the volume of the sample in wet state [37].

Similarly, the equilibrium mass swelling ratio was calculated as

$$SR = \frac{m_{swollen} - m_{dry}}{m_{dry}}, \quad (3)$$

where $m_{swollen}$ is the weight of swollen and m_{dry} is the weight of dry fibrous mat.

2.4.7. Permeability. Permeability of PVP and nCel/PVP fibrous mats (120–250 μm thickness) was determined according to Darcy's law [38] as

$$k_D = \frac{\mu h Q}{A \Delta P}, \quad (4)$$

where h is the fibrous mat thickness in meters, Q is the air flow rate in m^3/s, A is the area in m^2, μ is the viscosity of air (1.847×10^{-5} Pa.s at 25°C), and ΔP is the pressure drop across the sample. The data for Q and ΔP were obtained using a custom open-end flow cell with a 10 mm diameter aperture for the sample placement. At least five specimens were used in each type of the test to assess the textural and transport properties.

3. Results and Discussion

The crystalline structure of nanocellulose particles was confirmed by wide-angle X-ray diffraction (WAXD) (Figure 1). The peak fitting procedure revealed the position of the maxima at 14.6° (1-10), 16.6° (110), 20.4°(102), 22.6° (200), and 34.6° (004) 2θ, which is characteristic to cellulose Iβ monoclinic structure normally found in plants and trees [39]. The strongest peak at 22.6° (200) for nanocellulose particles was slightly shifted from the 22.4° peak observed for a sample of microcrystalline α-cellulose. The (200) peak was used to evaluate the size of crystallographically ordered domains that was calculated 7.8 ± 0.5 nm in all three nanocellulose samples.

FTIR spectra confirmed the purity of used nanocellulose materials and absence of any significant spectral variations between the nanocellulose particles of different sizes and microcrystalline cellulose. The main absorption bands in all spectra in Figure 2 were observed at 1427, 1370, 1313, 1202, 1160, 1105, 1052, 1028, 999, 983, and 897 cm^{-1}, which are

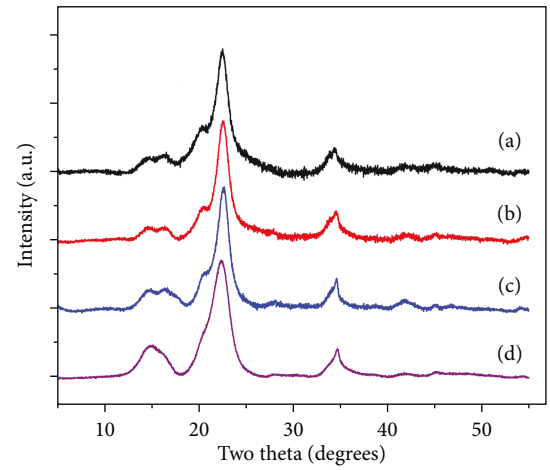

Figure 1: Wide-angle X-ray diffraction (WAXD) patterns of commercial (a) "ultra," (b) "natural," and (c) "thick" nanocellulose particle samples from Blue Goose Biorefineries Inc., in the comparison with (d) α-cellulose with 20 μm particle size (Sigmacell, Sigma-Aldrich).

characteristic peaks of type I cellulose. A broad band at 1642 cm^{-1} can be associated with adsorbed water in cellulose. The absorption band between 1427 cm^{-1} (indicated by arrow in Figure 2) is assigned to a symmetric CH_2 bending vibration, known as the "crystallinity band," and the band appearing at 897 cm^{-1} (indicated by arrow in Figure 2) is assigned to C–O–C stretching at β-(1→4)-glycosidic linkages, known as the "amorphous band" [40]. The ratio of 1427 cm^{-1} to 897 cm^{-1} band areas (lateral order index (LOI)) is correlated to the overall degree of order in the cellulose. The LOI was determined 1.67 for "ultra," 2.26 for "natural," 1.65 for "thick" types of nanocellulose, and 1.15 for α-microcellulose. The LOI numbers for nanocellulose particles are similar to those reported for cellulose from poplar wood feedstock [41] and other sources [42].

All three types of nanocellulose were successfully mixed with PVP solution with up to 1.0 : 8.0 nCel/PVP weight ratio, although the "natural" nanocellulose was the most challenging to mix. Figure 3(a) shows the variation of the nCel/PVP precursor viscosity depending on the concentration of PVP and cellulose particle size. A sharp increase in the viscosity has been noted in the "ultra" (smallest particle size) nCel/PVP precursor solution with 12 wt% PVP concentration. This increase was followed by the "natural" (medium particle size) nCel/PVP precursor, whereas the viscosity of the "thick" (largest particle size) nCel/PVP precursor was only slightly higher than that of pure PVP. The viscosity of all precursors declined in a similar manner with the increase in shear rate (Figure 3(a), insert) for all three tested concentrations (8, 10, and 12 wt% PVP). The shear thinning behavior can contribute to good spinnability of tested precursor solutions.

All nCel/PVP precursors with three PVP concentrations spun effectively. They all produced fairly thick (100–200 μm) layers of fibers with few droplets. The resulting fiber diameter (Figure 3(b)) was in the range from 300 to 2500 nm and followed closely the viscosity trends. The same trend was

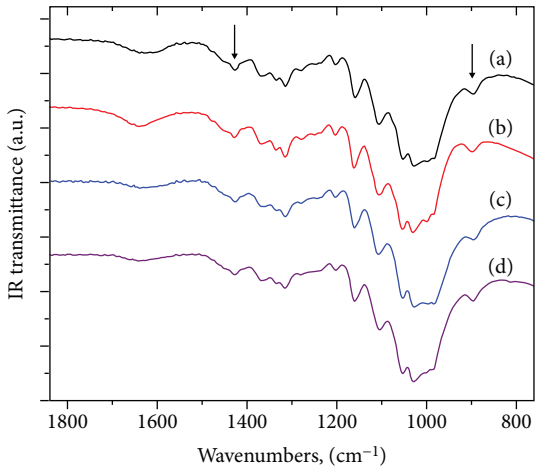

FIGURE 2: FTIR spectra of (a) "ultra," (b) "natural," and (c) "thick" nanocellulose particle samples in the comparison with (d) α-cellulose with 20 μm particle size.

also observed for pure PVP tested at the different concentrations. It was also noted that the precursors with the 1.0 : 8.0 nCel/PVP weight ratio spun more efficiently than did the precursors with less cellulose. This can be related to the effect of the increasing electric conductivity of precursors with more nCel content (Table 1).

All tested nCel/PVP and pure PVP fibers had a predominantly smooth surface morphology after the crosslinking (Figures 4(a)–4(d)). Pure PVP fibers were rather uniform and had almost no variation in diameter along their length. In nCel/PVP fibers, there were isolated thickened regions observed in a small fraction of fibers along their length. These regions can be best seen in the SEM image of "ultra" nCel/PVP fibers in Figure 4(a). The thickened regions can be associated with the presence of larger nanocellulose particles or with not fully dispersed particle aggregates inside the composite fibers. The uniformity of the fiber diameter generally increased when higher concentrations of precursors were used for each cellulose particle size. There was no evidence found in free nanocellulose particles, even for the largest, "thick" type, located between or attached to the surface of composite nanofibers. It can be concluded that at least "natural" (400–1200 nm long) and "thick" (700–2000 nm long) types of nanocellulose particles are fully integrated and aligned along the composite fiber length. The same can be assumed for "ultra" (100–200 nm long) nanocellulose particles. However, it has been reported [10] that the strong electric fields in the electrospinning process may not necessarily induce full orientation of nanocellulose particles inside the polymer matrix. It was observed that nanocellulose particles with 100 nm length and 6 nm width were mostly randomly oriented and only some local areas exhibited some orientation in PVA and polystyrene (PS) polymer fibers with up to 20% volume fraction of nanocellulose particle loading [10]. The nanocellulose particle misalignment can also affect the uniformity of the diameter and be responsible for formation of the thickened regions in nCel/PVP fibers (Figure 4(a)). Besides, the presence of the nanocellulose particle aggregates or large particles partially protruding from the liquid precursor droplet during the jet formation can create the local conditions for the formation of multiple jets. This can lead to the formation of very thin PVP fibers that contain either none or just a few random nanocellulose particles aligned along the fiber axis. Such thin fibers with the diameters comparable or smaller than those of individual nanocellulose particles (especially "thick" and "natural" type) can be seen in SEM images of all nCel/PVP fibers in Figures 4(a)–4(c).

Crosslinked nCel/PVP and pure PVP fibrous membranes were stable in DI water for at least one week. There was no mass loss detected, but the fibrous membrane microarchitecture was altered significantly (Figures 4(e)–4(h)). A noticeable fusion occurred between the fibers in pure PVP membranes, but the fiber shape and diameter were little affected (Figure 4(h)). All nCel/PVP samples showed strong deformation of the fibers, although only minor degree of fusion can be seen in the "ultra" nCel/PVP sample (Figure 4(e)). Such deformation can be associated with the difference in the residual stress in the interacting PVP and nCel components of the fibers after the nCel/PVP composite fibrous material dried from its wet swelled state.

FTIR spectra of as-prepared nCel/PVP fibers show several differences with the spectra of pure PVP fibers and nanocellulose particles (Figure 5). The strongest absorption band of PVP fibers (C=O/C–N stretching vibrations, centered at 1638 cm^{-1}, Figure 5(a)) loses its fine structure, and the maximum of absorption peak shifts to 1651–1655 cm^{-1} in the nCel/PVP composite fibers (Figures 5(b)–5(d)). Other PVP absorption bands do not show noticeable changes. Only three strongest absorption bands of nanocellulose can be resolved in the FTIR spectra of nCel/PVP fibers (indicated by arrows in Figure 5). The peak positions of all those bands were slightly shifted to higher frequencies from their positions in the precursor nanocellulose particles of all types. The peak at 1108 cm^{-1} (symmetric C–O–C glycosidic ether band stretching) is shifted from 1105 cm^{-1}, the peak at 1058 cm^{-1} (C–O stretching at C_3) is shifted from 1052 cm^{-1}, and the peak at 1033 cm^{-1} (C–O stretching at C_6) is shifted from 1028 cm^{-1} in the spectra of the precursor nanocellulose particles [43, 44]. Such band shifts indicate a certain level of interaction between PVP and cellulose molecules where PVP affects the H^+ bonding between the glycosidic link (C_5–O–C_1 group) and the hydroxyl group on C_3 of cellulose by eliminating this bond, which causes a small shift in the IR spectra of the mixtures.

To further understand the interaction of PVP with nanocellulose, DSC analysis of PVP and nCel/PVP fibers was performed in two heating cycles from room temperature to 200°C. DSC runs of as-prepared PVP and nCel/PVP fibers confirmed a significant amount of residual solvent vaporization, which gave rise to a broad endothermic peak observed in the first heating scan. Small endothermic peaks were noted in the region between 175 and 190°C in all nanofibrous samples (Figure 6). The glass transition temperature (T_g) of pure PVP fibers was determined at 177.5°C (onset) and 183°C (inflection point). The glass transition temperature typically reported for PVP K90 (MW1300000) is 177°C. There are no thermal events associated with cellulose in this temperature range [45].

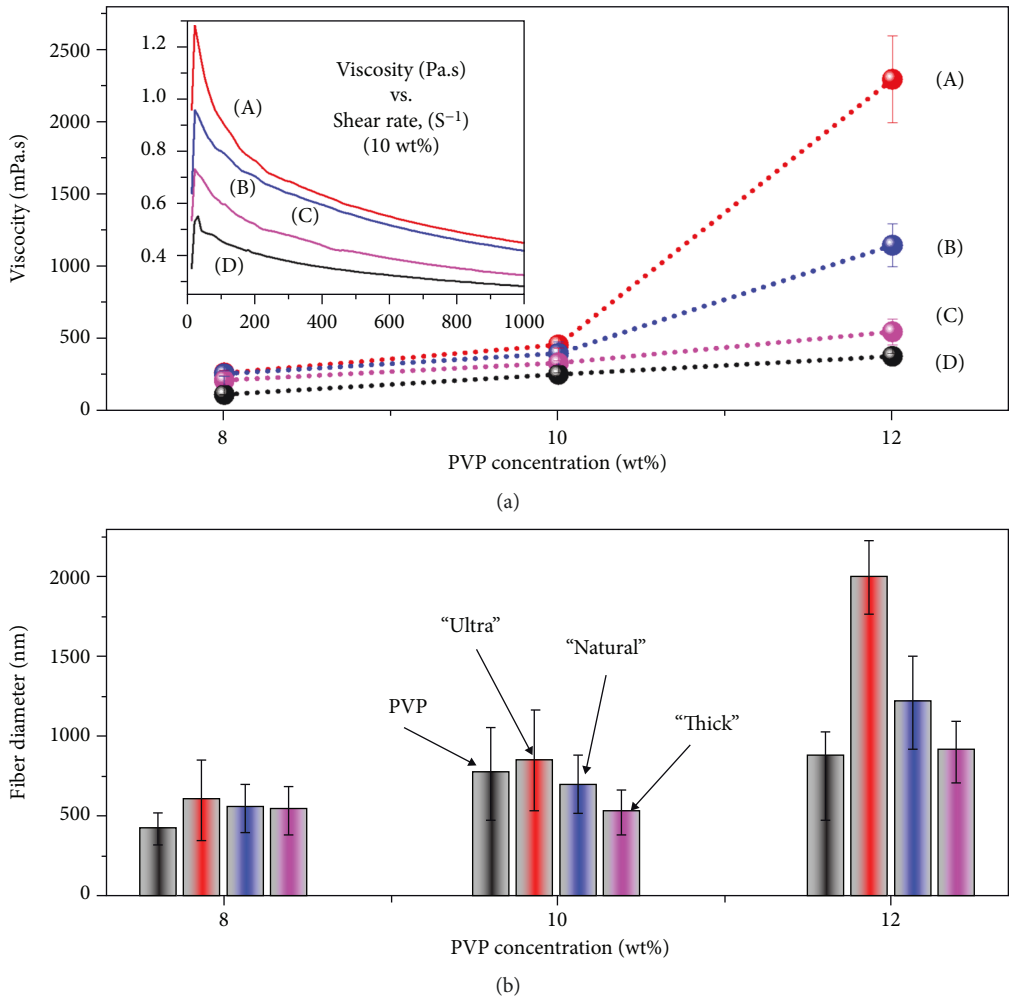

Figure 3: Dependence of viscosity (a) and fiber diameter (b) on the precursor concentration and composition: (A) "ultra," (B) "natural," (C) "thick" nCel/PVP with 1.0 : 8.0 weight ratio, and (D) pure PVP. Inset shows the change in viscosity with shear rate for pure PVP and nCel/PVP precursors with 10 w% PVP concentration.

However, it seems that the addition of nanocellulose slightly reduced the T_g of PVP to 176.7, 176.0, and 174.5°C (onset points in DSC traces in Figure 6) for the "thick," "natural," and "ultra" nanocellulose types, respectively. Cataldi et al. [46] noticed that a strong molecular interaction between nano- or microcellulose and the polymer matrix leads to higher T_g in composite materials. In the case of nCel/PVP fibrous material, the molecular interaction seems to be limited to hydrogen bonding, as suggested by FTIR spectra. The addition of nanocellulose particles can lead to the increased mobility of the amorphous polymer chains and reduction in T_g [12]. The glass transition temperature decreases gradually as the nanocellulose particle size becomes smaller, and it can be associated with a plasticization phenomenon [47].

Figure 7 presents the FTIR spectra of thermally crosslinked PVP and nCel/PVP fibers. After the thermal crosslinking, the FTIR spectrum of pure PVP fibers revealed a small peak at 1770 cm^{-1} and a shoulder centered around 1695 cm^{-1} in the 1650 cm^{-1} band (Figure 7(b), peaks are indicated by arrows). These spectral features are associated with the oxidative degradation of polymer at that temperature [48, 49]. Neither of these two spectral features was resolved in the spectra of nCel/PVP fibers (Figures 7(c)–7(e)). It has been also noted that the absorption peaks of nanocellulose were observed at 1105, 1055, and 1032 cm^{-1} (indicated by arrows in Figure 7), and thus, they were shifted by 2-3 cm^{-1} to lower frequencies from those observed in as-prepared nCel/PVP fibers. These peak positions became closer to those in FTIR spectra of the precursor nanocellulose particles (Figure 2). Besides, the PVP band observed around 1651–1655 cm^{-1} in as-prepared nCel/PVP fibers almost fully recovered its shape and position shifted back ~1640 cm^{-1} which was observed in as-prepared pure PVP fibers (Figure 7(a)). There were no changes noted in the position and intensity of other PVP peaks. The observed changes in FTIR spectra of thermally crosslinked nCel/PVP fibers can be associated with removal of hydrogen bonds that were initially formed between cellulose and PVP molecules. It has been also proposed that the presence of nanocellulose in PVP fibers increases the composite nanofiber stability to oxidation during the thermal crosslinking.

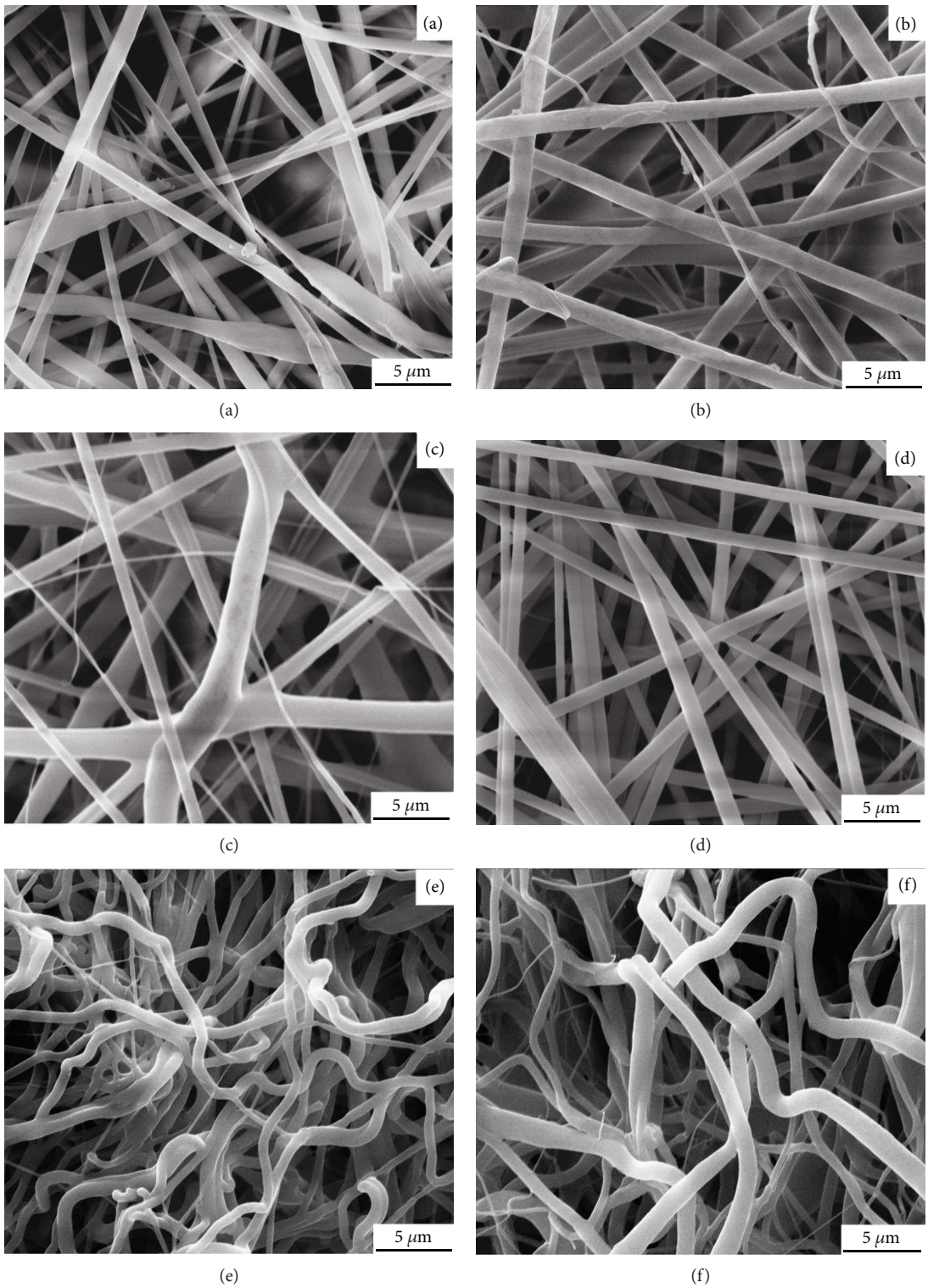

Figure 4: Continued.

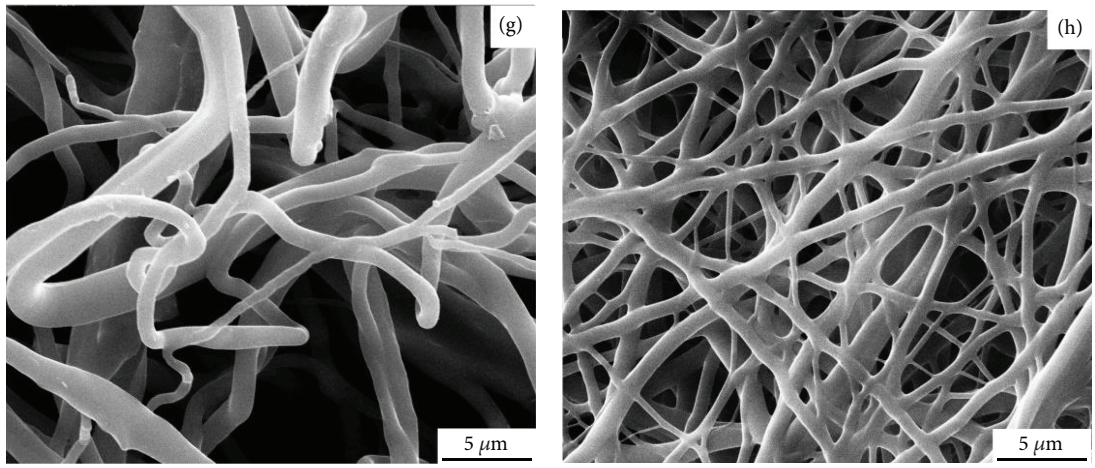

Figure 4: SEM images of crosslinked nCel/PVP fibrous mats prepared with (a)"ultra," (b) "natural," (c) "thick" type of nanocellulose and (d) pure PVP; (e–h) same fibrous mats after exposure in water for 1 week.

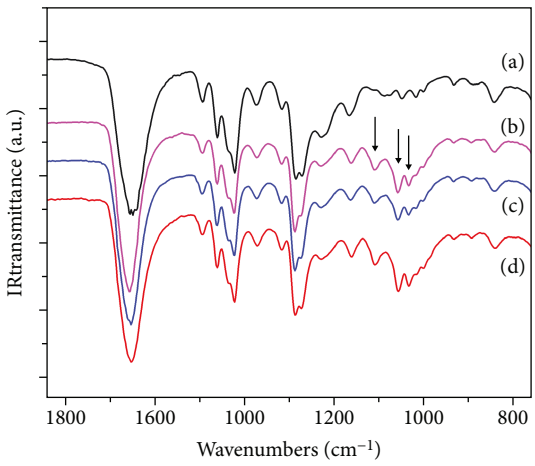

Figure 5: FTIR spectra of as-prepared (a) pure PVP, (b) "thick," (c) "natural," and (d) "ultra" nCel/PVP fibers with a 1.0 : 8.0 weight ratio.

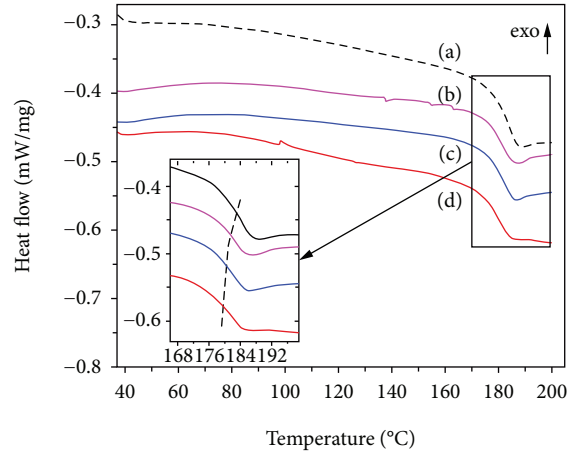

Figure 6: DSC traces (20°/min heating rate) for (a) pure PVP, (b) "thick," (c) "natural," and (d) "ultra" nCel/PVP fibers with a 1.0 : 8.0 weight ratio. The dotted line is to guide the reader's eye to the shift of inflection points in DSC traces.

Thermally crosslinked PVP and nCel/PVP fibrous mats with $100 \times 100\,mm^2$ area and thickness from 120 to 250 μm were prepared from the nCel/PVP precursor with 10 wt% PVP concentration and 1.0 : 8.0 nCel/PVP ratio to determine the effect of nanocellulose particle size on the bulk density, porosity, burst pressure, air transport, and swelling properties of the membranes fabricated from the electrospun mats. The nanofibrous mats were cut into $20 \times 20\,mm^2$ membranes, at least five such membranes were used in each test, and the results are summarized in Table 2. Taking the properties of the crosslinked pure PVP fibrous membrane as a basis, the "ultra" nCel/PVP fibrous material (smallest particle size) had most of the properties close to those of pure PVP fibrous material. The "ultra" nCel/PVP membranes exhibited a small increase in burst pressure that can be associated with the reinforcement effect of nanocellulose [22, 23] due to a higher level of intermolecular interaction between smaller nCel particles and PVP matrix in this case. However, this material had the lowest air permeability and mass swelling ratio when immersed in water, in comparison with all other materials. This can be related to a relatively higher density and rigidity of this structure. The "ultra" nCel/PVP membranes were noticeably brittle due to, perhaps, the highest residual stress level after they dried from the swelled wet state, when compared to other materials. Conversely, both "natural" and "thick" nCel/PVP membranes had a significantly higher porosity and Darcy's permeability coefficients but lower burst pressures than other two materials. The "natural" nCel/PVP membranes had the mass swelling ratio closest to pure PVP fibrous material, but the lowest burst pressure. Interestingly, the volume of the "natural" nCel/PVP membranes decreased due to a significant reduction in the membrane thickness in wet state while the membrane expanded laterally. All properties of the "thick" nCel/PVP fibrous membranes were between those for other materials. The observed differences can be due to several reasons. First,

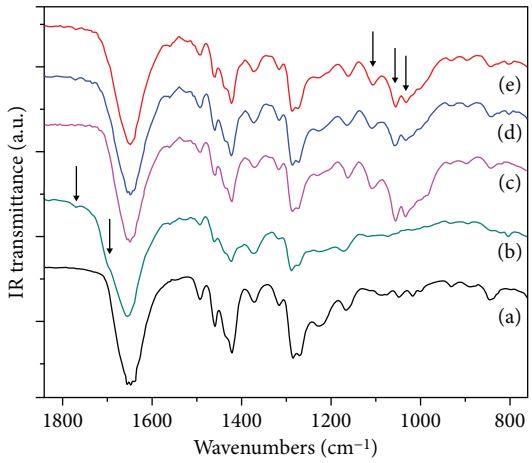

Figure 7: FTIR spectra of (a) as-prepared pure PVP, and thermally crosslinked at 200°C (b) pure PVP, (c) "thick," (d) "natural," and (e) "ultra" nCel/PVP fibers with a 1.0 : 8.0 weight ratio.

the production of composite fibers with "thick" and "natural" nanocellulose particles was faster than with "ultra" nanocellulose or with pure PVP. This leads to observed higher total porosity of the electrospun fibrous mats with larger fiber and pore diameters and to proportionally larger Darcy's permeability coefficients. More porous materials would usually have a lower mechanical strength. Second, larger nanocellulose particles may be aligned along the fiber axis but may not overlap fully inside the composite fibers. This can result in the PVP fiber segments without the nanocellulose particles, especially in smaller diameter fibers, which leads to a nonuniform distribution of nCel particles through the length of the fiber and a lower degree of the particle-matrix interaction. The changes in the position and fine features of the C=O/C–N infrared absorption band of PVP in "natural" and "thick" nCel/PVP fibers in FTIR spectra before and after the crosslinking, as well as DSC data, seem to support this assumption. The appearance of voids at the particle/matrix interface is also predicted for larger nCel particles, which can weaken the structure. The "natural" nCel suspension was the most difficult to mix with PVP solution, which probably led to the presence of such voids and to accordingly the lowest magnitude of burst pressure. A relatively soft, porous structure of "natural" and "thick" nCel/PVP fibrous membranes collapses easily in the direction normal to the plane of the membrane, but still holds well in plane due to the fibrous intertwined network when immersed in water. The differences in swelling of nanocellulose particle-rich and pure PVP fibrous segments can also add to residual stress levels in nCel and PVP components after the fibrous composite material dries. This can explain further the observed variations in the fiber shape (Figures 4(e)–4(g)), burst pressure, volume, and mass swelling ratio.

Darcy's air permeability tests conducted with nCel/PVP fibrous membranes (120–250 μm thickness) has shown that the permeability coefficient of "ultra" nCel/PVP membranes reduces slightly when pressure rises, but it increases for other two types of nCel/PVP materials (Figure 8). These changes are associated with the sample deformation that includes simultaneous compression and stretching of the fibrous mesh [50, 51]. At low pressure drop, the stretching dominates in pure PVP, "natural" and "thick" nCel/PVP fibrous membranes, which leads to increasing pore size and air transport. This was followed by the membrane compression at higher pressures, and a relatively steady state was reached. The "ultra" nCel/PVP fibrous membrane was noticeably stiffer than other materials due to a somewhat increased degree of fiber-fiber interaction in a denser as-spun material with smaller fiber diameters (Figure 4(e)), and it can stretch to a lesser degree that led to an observed behavior. The observed behavior of tested fibrous membrane structures is consistent with other properties discussed above. When an equilibrium state was reached, the nearly constant permeability with increasing pressure was observed in all cases until the membranes failed.

4. Conclusions

This study demonstrated that nCel/PVP fibrous materials with varied microarchitectures and properties can be prepared by DC electrospinning when using rod-like nanocellulose particles of different sizes. Regardless of the nanocellulose particle size, the nCel/PVP precursor solutions with up to 1.0 : 8.0 nCel/PVP ratios represented non-Newtonian fluids and they were readily spinnable using a capillary needle in a wide range of precursor and process parameters. The size of cellulose nanoparticle had a strong effect on the precursor viscosity, efficiency of the process, resulting fiber diameter, and properties of fabricated nCel/PVP fibrous membrane structures.

Hydrogen bonding occurred between nanocellulose and PVP molecules in electrospun fibers. The interaction between the nanocellulose and PVP increases when the cellulose particle size reduces. Despite this, the degree of interaction is relatively low as follows from a slight reduction in T_g of PVP as well as from small shifts of the absorption bands of cellulose and PVP in the FTIR spectra.

Electrospun nCel/PVP fibrous composite materials can be thermally crosslinked without noticeable changes in the dimensions of nanofibrous mat and fiber diameter. The addition of nanocellulose increases the thermal stability of PVP to oxidation, regardless of the particle size. The thermally crosslinked nCel/PVP fibrous materials exhibit the textural air transport and mass swelling properties that can vary significantly depending on the size of nanocellulose particles. Within the range of the tested precursor and electrospinning process parameters, the addition of nanocellulose particles with the smallest size resulted in some improvement in the strength of the crosslinked fibrous membranes during the air permeability tests but decreased its mass swelling capacity, whereas the nanocellulose particles with larger sizes led to a more porous, flexible, and swellable but mechanically weaker structure of the crosslinked fibrous membranes. It can, therefore, be predicted that by using the nanocellulose particles of different size and shape, the properties of electrospun and crosslinked nCel/PVP fibrous composites can be tailored to a specific application.

Table 2: Summary of select properties of electrospun and thermally crosslinked nCel/PVP and pure PVP fibrous membranes with 200 ± 40 μm thickness prepared from precursors with 10 wt% PVP and 1.0 : 8.0 nCel/PVP ratio.

Material	Average fiber diameter (nm)	Bulk density (g/cm^3)	Porosity dry (%)	Darcy's permeability, air (m^2)	Burst pressure, kPa, for 200 μm	Volume change in wet state (%)	Porosity wet (%)	Mass swelling ratio
"Ultra"/PVP	846	0.38	70.5	6.92×10^{-15}	20.0 ± 3.0	+21	76	2.42
"Natural"/PVP	702	0.19	85.3	6.92×10^{-13}	6.0 ± 1.5	-17	81.9	3.58
"Thick"/PVP	516	0.26	79.8	1.09×10^{-13}	8.0 ± 1.5	-2	79.7	3.03
PVP	835	0.35	72.2	8.35×10^{-15}	18.0 ± 3.0	+68	83.3	3.85

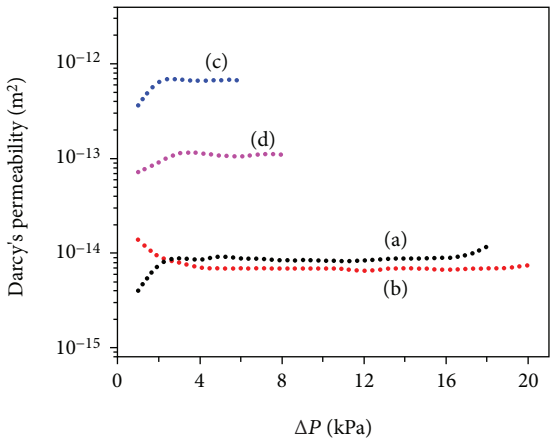

Figure 8: Darcy's permeability for air as a function of differential pressure of thermally crosslinked (a) "ultra," (b) "natural," (c) "thick" nCel/PVP fibrous membranes with a 1.0 : 8.0 cellulose/PVP weight ratio, and (d) PVP fibrous membrane.

Data Availability

The data used to support the findings of this study are available from the corresponding author upon request.

Conflicts of Interest

The authors declare that there is no conflict of interest regarding the publication of this paper.

Acknowledgments

Katrina Hatch is thankful for the support from the National Science Foundation International Research Experience for Students (IRES) Program (Grant #OISE-1558268). The authors thank Dr. Mike Hawkridge from PANalytical for the help with WAXD measurements and Dr. David Lukas for fruitful discussions.

References

[1] M. Jorfi and E. J. Foster, "Recent advances in nanocellulose for biomedical applications," *Journal of Applied Polymer Science*, vol. 132, no. 14, 2015.

[2] N. Lin and A. Dufresne, "Nanocellulose in biomedicine: current status and future prospect," *European Polymer Journal*, vol. 59, pp. 302–325, 2014.

[3] T. Abitbol, A. Rivkin, Y. Cao et al., "Nanocellulose, a tiny fiber with huge applications," *Current Opinion in Biotechnology*, vol. 39, pp. 76–88, 2016.

[4] K. Y. Lee, Y. Aitomäki, L. A. Berglund, K. Oksman, and A. Bismarck, "On the use of nanocellulose as reinforcement in polymer matrix composites," *Composites Science and Technology*, vol. 105, pp. 15–27, 2014.

[5] T. Subbiah, G. S. Bhat, R. W. Tock, S. Parameswaran, and S. S. Ramkumar, "Electrospinning of nanofibers," *Journal of Applied Polymer Science*, vol. 96, no. 2, pp. 557–569, 2005.

[6] D. H. Reneker, A. L. Yarin, E. Zussman, and H. Xu, "Electrospinning of nanofibers from polymer solutions and melts," *Advances in Applied Mechanics*, vol. 41, pp. 43–346, 2007.

[7] J. D. Schiffman and C. L. Schauer, "A review: electrospinning of biopolymer nanofibers and their applications," *Polymer Reviews*, vol. 48, no. 2, pp. 317–352, 2008.

[8] L. Persano, A. Camposeo, C. Tekmen, and D. Pisignano, "Industrial upscaling of electrospinning and applications of polymer nanofibers: a review," *Macromolecular Materials and Engineering*, vol. 298, no. 5, pp. 504–520, 2013.

[9] S. Huan, L. Bai, W. Cheng, and G. Han, "Manufacture of electrospun all-aqueous poly (vinyl alcohol)/cellulose nanocrystal composite nanofibrous mats with enhanced properties through controlling fibers arrangement and microstructure," *Polymer*, vol. 92, pp. 25–35, 2016.

[10] N. D. Wanasekara, R. P. O. Santos, C. Douch, E. Frollini, and S. J. Eichhorn, "Orientation of cellulose nanocrystals in electrospun polymer fibres," *Journal of Materials Science*, vol. 51, no. 1, pp. 218–227, 2016.

[11] C. Zhou, R. Chu, R. Wu, and Q. Wu, "Electrospun polyethylene oxide/cellulose nanocrystal composite nanofibrous mats with homogeneous and heterogeneous microstructures," *Biomacromolecules*, vol. 12, no. 7, pp. 2617–2625, 2011.

[12] S. Pirani, H. M. N. Abushammala, and R. Hashaikeh, "Preparation and characterization of electrospun PLA/nanocrystalline cellulose-based composites," *Journal of Applied Polymer Science*, vol. 130, no. 5, pp. 3345–3354, 2013.

[13] C. Zhou, Q. Shi, W. Guo et al., "Electrospun bionanocomposite scaffolds for bone tissue engineering by cellulose nanocrystals reinforcing maleic anhydride grafted PLA," *ACS Applied Materials and Interfaces*, vol. 5, no. 9, pp. 3847–3854, 2013.

[14] C. Zhang, M. R. Salick, T. M. Cordie, T. Ellingham, Y. Dan, and L. S. Turng, "Incorporation of poly(ethylene glycol) grafted cellulose nanocrystals in poly(lactic acid) electrospun nanocomposite fibers as potential scaffolds for bone tissue engineering," *Materials Science and Engineering: C*, vol. 49, pp. 463–471, 2015.

[15] Q. Shi, C. Zhou, Y. Yue, W. Guo, Y. Wu, and Q. Wu, "Mechanical properties and in vitro degradation of electrospun bionanocomposite mats from PLA and cellulose nanocrystals," *Carbohydrate Polymers*, vol. 90, no. 1, pp. 301–308, 2012.

[16] H. Y. Mi, X. Jing, J. Peng, M. R. Salick, X. F. Peng, and L. S. Turng, "Poly(ε-caprolactone) (PCL)/cellulose nano-crystal (CNC) nanocomposites and foams," *Cellulose*, vol. 21, no. 4, pp. 2727–2741, 2014.

[17] K. Sutjarittangtham, T. Tunkasiri, P. Chantawannakul, U. Intatha, and S. Eitssayeam, "Mechanically improved antibacterial polycaprolactone/propolis electrospun fiber mat by adding bacterial nanocellulose," *Journal of Computational and Theoretical Nanoscience*, vol. 12, no. 5, pp. 798–803, 2015.

[18] J. Si, Z. Cui, Q. Wang, Q. Liu, and C. Liu, "Biomimetic composite scaffolds based on mineralization of hydroxyapatite on electrospun poly(ε-caprolactone)/nanocellulose fibers," *Carbohydrate Polymers*, vol. 143, pp. 270–278, 2016.

[19] Y. Mo, R. Guo, J. Liu et al., "Preparation and properties of PLGA nanofiber membranes reinforced with cellulose nanocrystals," *Colloids and Surfaces B: Biointerfaces*, vol. 132, pp. 177–184, 2015.

[20] K. Paulett, W. A. Brayer, K. Hatch et al., "Effect of nanocrystalline cellulose addition on needleless alternating current electrospinning and properties of nanofibrous polyacrylonitrile meshes," *Journal of Applied Polymer Science*, vol. 135, no. 5, 2018.

[21] M. S. Peresin, Y. Habibi, J. O. Zoppe, J. J. Pawlak, and O. J. Rojas, "Nanofiber composites of polyvinyl alcohol and cellulose nanocrystals: manufacture and characterization," *Biomacromolecules*, vol. 11, no. 3, pp. 674–681, 2010.

[22] S. Huang, L. Zhou, M. C. Li, Q. Wu, Y. Kojima, and D. Zhou, "Preparation and properties of electrospun poly (vinyl pyrrolidone)/cellulose nanocrystal/silver nanoparticle composite fibers," *Materials*, vol. 9, no. 7, p. 523, 2016.

[23] R. J. Going, D. E. Sameoto, and C. Ayranci, "Cellulose nanocrystals: dispersion in co-solvent systems and effects on electrospun polyvinylpyrrolidone fiber mats," *Journal of Engineered Fibers and Fabrics*, vol. 10, no. 3, pp. 155–163, 2018.

[24] R. Balgis, H. Murata, Y. Goi, T. Ogi, K. Okuyama, and L. Bao, "Synthesis of dual-size cellulose-polyvinylpyrrolidone nanofiber composites via one-step electrospinning method for high-performance air filter," *Langmuir*, vol. 33, no. 24, pp. 6127–6134, 2017.

[25] N. Roy, N. Saha, P. Humpolicek, and P. Saha, "Permeability and biocompatibility of novel medicated hydrogel wound dressings," *Soft Materials*, vol. 8, no. 4, pp. 338–357, 2010.

[26] N. Roy and N. Saha, "PVP-based hydrogels: synthesis, properties and applications," in *Hydrogels: Synthesis, Characterization and Applications*, F. V. Câmara and L. J. Ferreira, Eds., pp. 227–252, Nova Science, Hauppauge, NY, USA, 2012.

[27] X. Y. Dai, W. Nie, Y. C. Wang, Y. Shen, Y. Li, and S. J. Gan, "Electrospun emodin polyvinylpyrrolidone blended nanofibrous membrane: a novel medicated biomaterial for drug delivery and accelerated wound healing," *Journal of Materials Science: Materials in Medicine*, vol. 23, no. 11, pp. 2709–2716, 2012.

[28] G. S. Irmukhametova, E. M. Shaikhutdinov, R. K. Rakhmetullayeva et al., "Nanostructured hydrogel dressings on base of crosslinked polyvinylpyrrolidone for biomedical application," *Advanced Materials Research*, vol. 875-877, pp. 1467–1471, 2014.

[29] D. Lubasova, H. Niu, X. Zhao, and T. Lin, "Hydrogel properties of electrospun polyvinylpyrrolidone and polyvinylpyrrolidone/poly(acrylic acid) blend nanofibers," *RSC Advances*, vol. 5, no. 67, pp. 54481–54487, 2015.

[30] Q. G. Zhang, W. W. Hu, A. M. Zhu, and Q. L. Liu, "UV-cross-linked chitosan/polyvinylpyrrolidone blended membranes for pervaporation," *RSC Advances*, vol. 3, no. 6, pp. 1855–1861, 2013.

[31] M. Fujii, H. Okada, Y. Shibata, H. Teramachi, M. Kondoh, and Y. Watanabe, "Preparation, characterization, and tableting of a solid dispersion of indomethacin with crospovidone," *International Journal of Pharmaceutics*, vol. 293, no. 1-2, pp. 145–153, 2005.

[32] P. Verheyen, K. J. Steffens, and P. Kleinebudde, "Use of crospovidone as pelletization aid as alternative to microcrystalline cellulose: effects on pellet properties," *Drug Development and Industrial Pharmacy*, vol. 35, no. 11, pp. 1325–1332, 2009.

[33] S. M. Shaddy, M. A. Arnold, K. Shilo et al., "Crospovidone and microcrystalline cellulose: a novel description of pharmaceutical fillers in the gastrointestinal tract," *American Journal of Surgical Pathology*, vol. 41, no. 4, pp. 564–569, 2017.

[34] W. G. Glasser, R. H. Atalla, J. Blackwell et al., "About the structure of cellulose: debating the Lindman hypothesis," *Cellulose*, vol. 19, no. 3, pp. 589–598, 2012.

[35] B. Medronho, A. Romano, M. G. Miguel, L. Stigsson, and B. Lindman, "Rationalizing cellulose (in)solubility: reviewing basic physicochemical aspects and role of hydrophobic interactions," *Cellulose*, vol. 19, no. 3, pp. 581–587, 2012.

[36] L. Segal, J. J. Creely, A. E. Martin Jr., and C. M. Conrad, "An empirical method for estimating the degree of crystallinity of native cellulose using the X-ray diffractometer," *Textile Research Journal*, vol. 29, no. 10, pp. 786–794, 1959.

[37] A. Roy, P. Bhunia, and S. De, "Solvent effect and macrovoid formation in cellulose acetate phthalate (CAP)–polyacrylonitrile (PAN) blend hollow fiber membranes," *Journal of Applied Polymer Science*, vol. 134, no. 1, 2017.

[38] F. Dullien, *Porous Media – Fluid Transport and Pore Structure*, Academic Press, New York, NY, USA, 1979.

[39] R. J. Moon, T. Pöohler, and T. Tammelin, "Microscopic characterization of nanofibers and nanocrystals," in *Handbook of Green Materials: Processing Technologies, Properties and Applications*, K. Oksman, A. P. Mathew, A. Bismarck, O. Rojas, and M. Sain, Eds., pp. 159–180, World Scientific, Hackensack, NJ, USA, 2014.

[40] M. L. Nelson and R. T. O'Connor, "Relation of certain infrared bands to cellulose crystallinity and crystal lattice type. Part II. A new infrared ratio for estimation of crystallinity in celluloses I and II," *Journal of Applied Polymer Science*, vol. 8, no. 3, pp. 1325–1341, 1964.

[41] T. Auxenfans, D. Crônier, B. Chabbert, and G. Paës, "Understanding the structural and chemical changes of plant biomass following steam explosion pretreatment," *Biotechnology for Biofuels*, vol. 10, no. 1, p. 36, 2017.

[42] M. Poletto, H. Ornaghi Jr., and A. Zattera, "Native cellulose: structure, characterization and thermal properties," *Materials*, vol. 7, no. 9, pp. 6105–6119, 2014.

[43] E. H. Qua, P. R. Hornsby, H. S. S. Sharma, G. Lyons, and R. D. McCall, "Preparation and characterization of poly(vinyl alcohol) nanocomposites made from cellulose nanofibers," *Journal of Applied Polymer Science*, vol. 113, no. 4, pp. 2238–2247, 2009.

[44] S. Y. Oh, D. I. Yoo, Y. Shin et al., "Crystalline structure analysis of cellulose treated with sodium hydroxide and carbon dioxide by means of X-ray diffraction and FTIR spectroscopy," *Carbohydrate Research*, vol. 340, no. 15, pp. 2376–2391, 2005.

[45] L. Szcześniak, A. Rachocki, and J. Tritt-Goc, "Glass transition temperature and thermal decomposition of cellulose powder," *Cellulose*, vol. 15, no. 3, pp. 445–451, 2008.

[46] A. Cataldi, L. Berglund, F. Deflorian, and A. Pegoretti, "A comparison between micro- and nanocellulose-filled composite adhesives for oil paintings restoration," *Nanocomposites*, vol. 1, no. 4, pp. 195–203, 2015.

[47] K. Halász and L. Csóka, "Plasticized biodegradable poly(lactic acid) based composites containing cellulose in micro- and nanosize," *Journal of Engineering*, vol. 2013, Article ID 329379, 9 pages, 2013.

[48] K. Uetani, T. Okada, and H. T. Oyama, "Crystallite size effect on thermal conductive properties of nonwoven nanocellulose sheets," *Biomacromolecules*, vol. 16, no. 7, pp. 2220–2227, 2015.

[49] T. E. Newsome and S. V. Olesik, "Electrospinning silica/polyvinylpyrrolidone composite nanofibers," *Journal of Applied Polymer Science*, vol. 131, no. 21, 2014.

[50] L. T. Choong, Z. Khan, and G. C. Rutledge, "Permeability of electrospun fiber mats under hydraulic flow," *Journal of Membrane Science*, vol. 451, pp. 111–116, 2014.

[51] P. W. Gibson, K. Desabrais, and T. Godfrey, "Dynamic permeability of porous elastic fabrics," *Journal of Engineered Fibers and Fabrics*, vol. 7, Supplement 2, pp. 29–36, 2018.